Applied Thermal Engineering 29 (2009) 1058–1066

Contents lists available at ScienceDirect

Applied Thermal Engineering

journal homepage: www.elsevier.com/locate/apthermeng

Mathematical model of bypass behaviors used in scroll compressor

Yangguang Liu [a], Chinghua Hung [a,*], Yuchoung Chang [b]

[a] Department of Mechanical Engineering, National Chiao Tung University, EE452, 1001 Ta Hsueh Road, Hsinchu 300, Taiwan
[b] Energy and Environment Research Laboratories, Industrial Technology Research Institute, Taiwan

ARTICLE INFO

Article history:
Received 11 February 2008
Accepted 19 May 2008
Available online 5 June 2008

Keywords:
Bypass
Valves
Scroll compressor
Efficiency

ABSTRACT

This paper has constructed a bypass mechanism mathematical model in scroll-type compressor (STC) and has been integrated into a simulation package to predict the STC performance. The bypass mechanism, when added to a fixed scroll, is used to prevent over-compression and liquid slugging. Under five specified operating conditions, it was found that the STC with the bypass action increased the isentropic efficiency 2.5–10% more than the STC without the bypass action. Meanwhile, the calculated results of the developed model have been validated by a STC testing apparatus. In addition, it was found that the design of the bypass mechanism in the paper, can completely avoid over-compression and pressure discrepancy while the STC is in operation.
© 2008 Elsevier Ltd. All rights reserved.

1. Introduction

The scroll-type compressor (STC) of variable pressure ratio was developed in recent years due to higher efficiency and power saving considerations. The pressure ratio is defined as the ratio of the saturated condenser pressure to the saturated evaporator pressure ($\frac{P_{dis}}{P_s}$), and is decided by operating conditions.

In general, volume ratio is fixed after the geometrical parameters of the STC have been decided. When the pressure ratio does not match with the volume ratio of the STC, two cases, over-compression and under-compression, will happen [1]. For under-compression, the repetitive compression in the final chamber or back flow from discharge chamber will occur in different designs of STC. For over-compression, the STC will compress the gas to its design point regardless of the high pressure in chambers and extra work is consumed. Under-compression could not be avoided except by designing a STC with low volume ratio while narrowing the range of operating conditions. Nevertheless, over-compression could be reduced by using bypass valves added to the fixed scroll.

Discussions of bypass valves of STC are seldom seen in papers but have been presented in several patents. Murayama et al. [2] designed two groups of bypass holes for each compression chamber with valves operated by pressure to prevent over-compression. Fuji et al. [3] use a plurality of symmetrical bypass holes to avoid over-compression caused by the open delay of the bypass valves. A STC with a back pressure mechanism for axial seal and bypass valves for over-compression is also exposed [4]. In addition, a study using bypass mechanism and optimization of the volume ratio in STC was presented to improve efficiency by 10–20% under the conditions of both low speed and low pressure ratio [5]. Even so, the examples above merely illustrated the design of bypass valves with abbreviated drawings and brief statements. They do not disclose the detailed mathematical models of the bypass mechanism, such as the selection of the position of bypass holes, valve models, and the bypass behavior during the compression and discharge process.

This paper constructs a general bypass valves model and integrates it into an already developed STC package [6]. Through the simulation results, the effects of bypass mechanism in the STC are investigated. The reliability and accuracy of this model were verified by the experimental test platform for an actual STC product using CO_2 as refrigerant.

2. Mathematical models

The whole mathematical models of STC include the geometry of the scroll, thermodynamics with refrigerant in compression and discharge processes, leakage through clearances, back pressure mechanism, superheat of suction pipe, and dynamic balance of mechanical components. For simplicity, some assumptions must be employed in the models:

(1) Refrigerant in working chambers is homogeneous.
(2) Gravitational, kinetic energy variations are neglected.
(3) Oil effects are neglected.
(4) Chambers of the scroll pairs are symmetrical.
(5) The bypass holes are located at fixed scroll.

2.1. Geometrical model of scrolls

The profiles of a pair of scrolls in the study are created by an involute with base circle. Equations of a fixed scroll can be written as follows:

* Corresponding author. Tel.: +886 3 5712121 55160; fax: +886 3 5720634.
E-mail addresses: ygliu.me94g@nctu.edu.tw (Y. Liu), chhung@mail.nctu.edu.tw (C. Hung).

1359-4311/$ - see front matter © 2008 Elsevier Ltd. All rights reserved.
doi:10.1016/j.applthermaleng.2008.05.023

Nomenclature

A	area (m^2)
A_{By}	uncovered cross-section area (m^2)
C	coefficient (−)
C_{valve}	spring constant of valve (N m^{-1})
CC_1	convergence criterion (−)
d	distance between wrap profile and center of bypass hole (m)
d_{tu}	tube diameter (m)
f	flow friction factor (m)
G	refrigerant mass flow rate (kg min^{-1})
h	height (m)
h_{tu}	coefficient of heat convection (W m^{-2} K^{-1})
L_i	length of the inner involute (m)
L_o	length of the outer involute (m)
li	distance between inner involute and bypass hole center (m)
lo	distance between outer involute and bypass hole center (m)
$\dot{m}$	mass flow rate (kg s^{-1})
m	slope (−)
N, n	turn number of scrolls; polytropic index (−)
p, P	pressure (MPa); power (W)
Pr	Prandtl number (−)
p_t	pitch of scroll (m)
Re	Reynolds number (−)
r	radius of bypass hole (m)
r_b	basic radius (m)
r_{eq}	equal radius (m)
r_{ob}	orbiting radius (m)
t	thickness (m)
V	volume (m^3)
x, y	coordinate (−)

Greek symbols

α	initial angle of involute (°)
δ	clearance (m)
ϕ	involute angle of scroll (°)
θ	orbiting angle of scroll (°)
λ	coefficient of heat conductivity (W m^{-1} K^{-1})
ρ	density (kg m^{-3})
ω	rpm (rev min^{-1})

Subscripts

b	base circle
back	back-side
C, c	isentropic; current
dis	discharge
dw	downstream
e	end-side
eq	equivalent
f	flank
fi_i	inner involute of fixed scroll
fi_o	outer involute of fixed scroll
i	index number
in	inlet
l	leakage
l,c	current leakage
l,e	end side leakage
l,p	previous leakage
motor	motor
out	outlet
o_a	corresponding involute angle for bypass hole
o_By	Bypass hole coordinate to outer involute
o_l	lower limit of the outer involute angle for bypass hole
o_u	upper limit of the outer involute angle for bypass hole
ob_i	inner involute of orbiting scroll
ob_o	outer involute of orbiting scroll
r	roll angle of scroll
s	suction
s,h	superheat
t	tangent coordinate
up	upstream
V	volumetric

$$x_{fi\_o} = r_b[\cos\phi + (\phi - \alpha)\sin\phi]$$
$$y_{fi\_o} = r_b[\sin\phi - (\phi - \alpha)\cos\phi] \quad (1)$$
$$x_{fi\_i} = r_b[\cos\phi + (\phi + \alpha)\sin\phi]$$
$$y_{fi\_i} = r_b[\sin\phi - (\phi + \alpha)\cos\phi] \quad (2)$$

Some fundamental calculations were derived from the papers [7,8].

2.2. Geometry of bypass holes

The scroll pairs were divided into several symmetrical chambers initially as shown in Fig. 1a. The relation of bypass holes between fixed scroll and orbiting scroll during the orbiting operation can be derived by using coordinates transformation.

2.2.1. Corresponding angle of the orbiting scroll

First, the range of one bypass hole's position (Fig. 1a) with outer profile (1) on the fixed scroll is considered as follows:

$$\phi_{o\_u} \geqslant \phi_{o\_a} \geqslant \phi_{o\_l}$$
$$\text{When } \phi_{o\_u} > 2\pi, \begin{cases} \phi_{o\_u} = \phi_r - \pi - (N-i)2\pi : i = 1,2,\ldots,N \\ \phi_{o\_l} = \phi_{o\_u} - 2\pi \end{cases} \quad (3)$$
$$\text{When } \phi_{o\_u} \leqslant 2\pi, \begin{cases} \phi_{o\_u} = \phi_r - \pi - (N-i)2\pi : i = 1,2,\ldots,N \\ \phi_{o\_l} = 0 \end{cases}$$

After the involute angle ϕ_{o_a} is defined, the other two parameters, r and d, shown in Fig. 1b, as constraints must be satisfied as follows:

$$\begin{cases} 0 \leqslant r \leqslant t/2 \\ r \leqslant d \leqslant p_t - t - r \end{cases} \quad (4)$$

It is important to provide reasonable values to assure the simulated results are physically meaningful.

Secondly, by observing Fig. 1b, the center of the bypass hole can be derived accordingly. Letting the slope m as:

$$\begin{cases} x_t = r_b\cos\phi_{o\_a} \\ y_t = r_b\sin\phi_{o\_a} \end{cases} \quad (5)$$
$$m = \frac{(y_{o\_a} - y_t)}{(x_{o\_a} - x_t)}$$

The center of the bypass hole at the fixed scroll is:

$$\begin{cases} x_{o\_By} = x_{o\_a} + d\cos(\tan^{-1} m) \\ y_{o\_By} = y_{o\_a} + d\sin(\tan^{-1} m) \end{cases} \quad (6)$$

Then the line equation from the tangential of basic circle of the fixed scroll to the center of bypass hole was derived as:

$$y = m(x - x_{o\_By}) + y_{o\_By} \quad (7)$$

The equations of the inner profile of the orbiting scroll and (7) are considered simultaneously as:

$$y = m(x - x_{o\_By}) + y_{o\_By}$$
$$\begin{cases} x = -r_b[\cos\phi + (\phi - \alpha)\sin\phi] + r_{ob}\cos\theta \\ y = -r_b[\sin\phi - (\phi - \alpha)\cos\phi] - r_{ob}\sin\theta \end{cases} \quad (8)$$

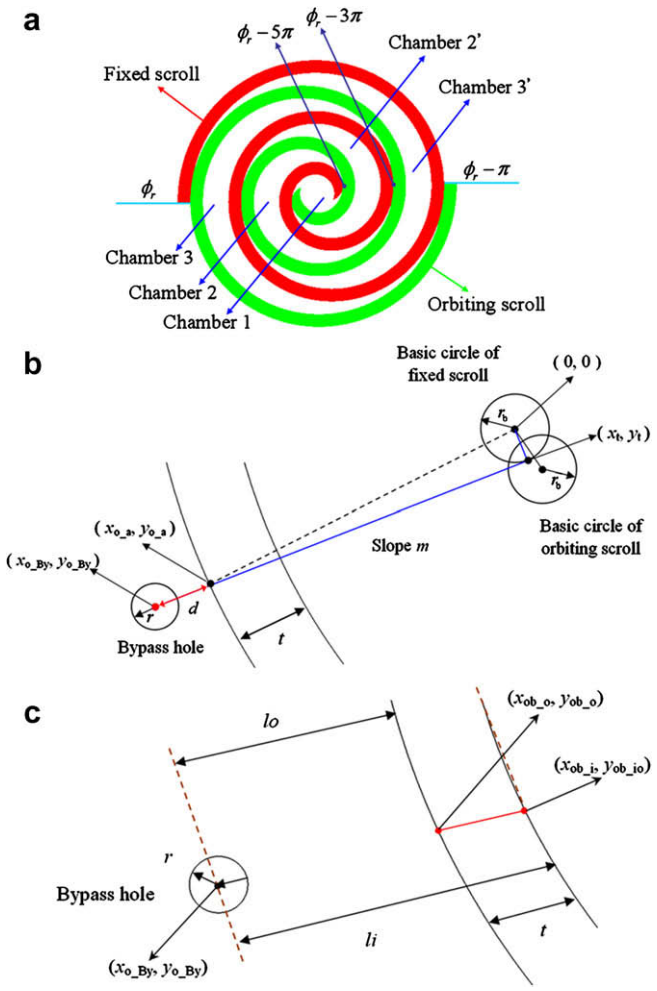

Fig. 1. Scheme of bypass holes (a) range of positions (b) relations from fixed scroll (c) relations from orbiting scroll.

Newton–Raphson method is used to solve these numerically and the corresponding involute angle ϕ on orbiting scroll can be obtained eventually.

2.2.2. Uncovered area of the bypass holes

While ϕ is determined, the relations between the center of the bypass hole and orbiting scroll profile can be defined as Fig. 1c. Therefore, two parameters lo and li are derived as:

$$\begin{aligned} \mathrm{lo} &= \sqrt{(x_{o\_By} - x_{ob\_o})^2 + (y_{o\_By} - y_{ob\_o})^2} \\ \mathrm{li} &= \sqrt{(x_{o\_By} - x_{ob\_i})^2 + (y_{o\_By} - y_{ob\_i})^2} \end{aligned} \tag{9}$$

These two parameters can be used to define the uncovered area of the bypass hole.

If lo < li holds, four possible calculations exist:

(A): As Condition (A) in Fig. 2, if li $\geqslant t + r$, then the uncovered area is

$$A_{By} = \pi r^2 \tag{10}$$

(B): As Condition (B) in Fig. 2, if li $\geqslant t$ and li $< t + r$, then

$$A_{By} = \left\{ \pi - \tan^{-1}\left[\frac{(r^2 - \mathrm{lo}^2)^{0.5}}{\mathrm{lo}} \right] \right\} r^2 + \mathrm{lo}(r^2 - \mathrm{lo}^2)^{0.5} \tag{11}$$

(C) As Condition (C) in Fig. 2, if li $\geqslant t - r$ and li $< t$, then

$$A_{By} = r^2 \tan^{-1}\left[\frac{(r^2 - \mathrm{lo}^2)^{0.5}}{\mathrm{lo}} \right] - \mathrm{lo}(r^2 - \mathrm{lo}^2)^{0.5} \tag{12}$$

(D) As Condition (D) in Fig. 2, if li $\leqslant t - r$, then $A_{By} = 0$.

If lo > li, those calculations still hold if the definition of the two parameters are interchanged. Aside from the uncovered area of the bypass holes to the outer profile of the orbiting scroll, the calculation to the inner profile proceeds similarly.

2.2.3. Corresponding chambers to bypass holes

Due to the motion of the orbiting scroll, the bypass holes may span to different chambers during a cycle. Determination of

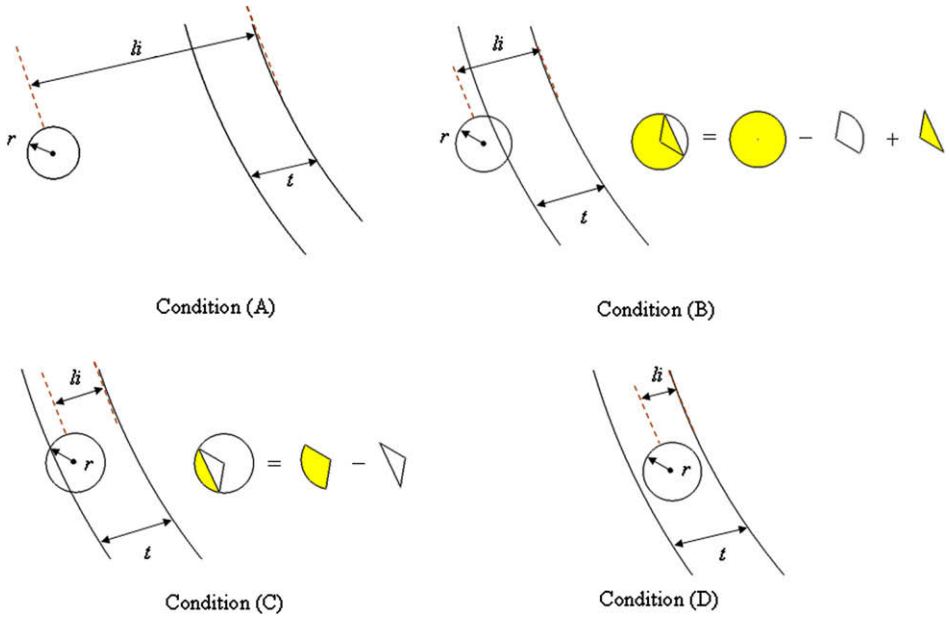

Fig. 2. Uncovered areas of the orbiting scroll and the bypass hole.

corresponding chambers to bypass holes must be performed. Observing the variations of the uncovered area of the bypass holes at current and previous steps during a cycle is a way to settle it.

2.3. Bypass valve model

A one-dimensional valve was used for simplicity [8] and the dynamics of the bypass valve was neglected. If the pressure in the compression chamber surpasses p_{dis}, the valve opens and the distance raised is determined with static forces balance relation:

$$y = \pi r_{eq}^2 (p - p_{dis}) \frac{1}{C_{valve}} \tag{13}$$

where r_{eq} is the equivalent radius for the uncovered area as follows:

$$r_{eq} = \left(\frac{A_{By}}{\pi}\right)^{0.5} \tag{14}$$

Then the equivalent flow area is calculated by

$$A_{eq} = 2\pi r_{eq} y \tag{15}$$

2.4. Compression process

The mass conservation of refrigerant in chambers during the compression process is

$$\dot{m} = \dot{m}_{in} - \dot{m}_{out} \tag{16}$$

The refrigerant state in the control volume can be described by a polytropic process [9] as follows:

$$p_c = p_s \left(\frac{\rho_c}{\rho_s}\right)^n \tag{17}$$

where n can be measured by laboratory experiment [10].

2.5. Refrigerant property

The Refprop 7 [11] published by NIST is a powerful tool that is used to obtain lots of data in thermodynamics for most refrigerants. This study integrates it by linking the dynamic link libraries to acquire the related properties.

2.6. Suction heating of the inlet refrigerant

The inlet refrigerant is heated by the suction pipe in the STC and the pipe is filled with refrigerant which flows out from the discharge chamber. The heat transfer coefficient for the pipe can be expressed by the Gnielinski relationship [12]:

$$h_{tu} = \frac{\lambda}{d_p} \times \frac{(f/8)(Re - 1000)Pr}{1 + 12.7\sqrt{f/8}(Pr^{2/3} - 1)} \tag{18}$$

Then the suction superheat can be evaluated.

2.7. Back-pressure mechanism

The back-pressure may be decided to be either proportional to p_s or p_{dis} [8]. Because p_s or p_{dis} changes with operating conditions, so the back-pressure would change, which would cause difficulties in designing a balanced mechanism to maintain suitable seal. Tsubono et al. [4] has shown that it is appropriate to treat back-pressure as proportional to p_s only, and the simplification was adopted in this study.

2.8. Leakage and bypass

Generally, end-side and flank leakage occur in the STC and can be shown as follow:

$$\dot{m}_l = \dot{m}_{l,e} + \dot{m}_{l,f} \tag{19}$$

where $\dot{m}_{l,e}$ and $\dot{m}_{l,f}$ are the end-side and flank leakage mass flow rates. Gap sizes of the two kinds of leakage are both dynamically related to pressure ratio [8] and back-pressure. The end-side gap δ_e, in meters, can be derived as shown below:

$$\delta_e = \left[1.02 \times \left(\frac{p_d - p_{back}}{p_s}\right) - 0.45\right] \times 10^{-6} \tag{20}$$

The end-side flow areas can be calculated [8] as

$$\begin{aligned} A_{in} &= \delta_e \int_{\phi_k}^{\phi_{k+1}} L_o \mathrm{d}\phi \\ A_{out} &= \delta_e \int_{\phi_k}^{\phi_{k+1}} L_i \mathrm{d}\phi \end{aligned} \tag{21}$$

where ϕ_{k+1} and ϕ_k are the involute angles of the conjugate end points for the scroll pair.

For end-side leakage, one-dimensional isentropic compressible flow [8] is used as

$$\begin{aligned} &\dot{m}_{l,e} = C \times A \left\{ p_{up} \times \rho_{up} \times \frac{2n}{n-1} \left[\left(\frac{p_{dw}}{p_{up}}\right)^{\frac{2}{n}} - \left(\frac{p_{dw}}{p_{up}}\right)^{\frac{n+1}{n}} \right] \right\}^{0.5} \\ &\text{when} \quad \left(\frac{p_{dw}}{p_{up}}\right) \geqslant \left(\frac{2}{n+1}\right)^{\frac{n}{n-1}}, \\ &\dot{m}_{l,e} = C \times A \left[p_{up} \times \rho_{up} \times n \times \left(\frac{2}{n+1}\right)^{\frac{n+1}{n-1}} \right]^{0.5} \\ &\text{when} \left(\frac{p_{dw}}{p_{up}}\right) < \left(\frac{2}{n+1}\right)^{\frac{n}{n-1}} \end{aligned} \tag{22}$$

where A is A_{in} or A_{out} for inflowing or outflowing conditions. Similarly, the flank gap is expressed in meters as follows:

$$\delta_f = \left[-6 \times \left(\frac{p_{dis} - p_{back}}{p_s}\right) + 20\right] \times 10^{-6} \tag{23}$$

The flank flow area [13] is

$$A_f = h\delta_f \tag{24}$$

For $\dot{m}_{l,f}$, Eq. (22) is also used with $A = A_f$. Then the total leakage mass flow rate can be calculated. In additions, the bypass flow rate can also be obtained by using Eq. (22) but substituting A with A_{eq}.

3. Computer model and simulation process

The simulation process with the computer package was developed by using C++ Builder, EXCEL and REFPROP 7. The inputs and outputs of the models and simulation process are described below.

3.1. Inputs

The inputs of the STC package include scroll geometry, related mechanisms, bypass valves, operating conditions and motor inputs that came from a dynamometer test.

3.2. Simulation process

The flowchart of the package is shown in Fig. 3a. The leakage and bypass model is included in the process and solved with numerical iterations. The flowchart of the leakage and bypass model is shown in Fig. 3b. When the pressure in the chamber is greater

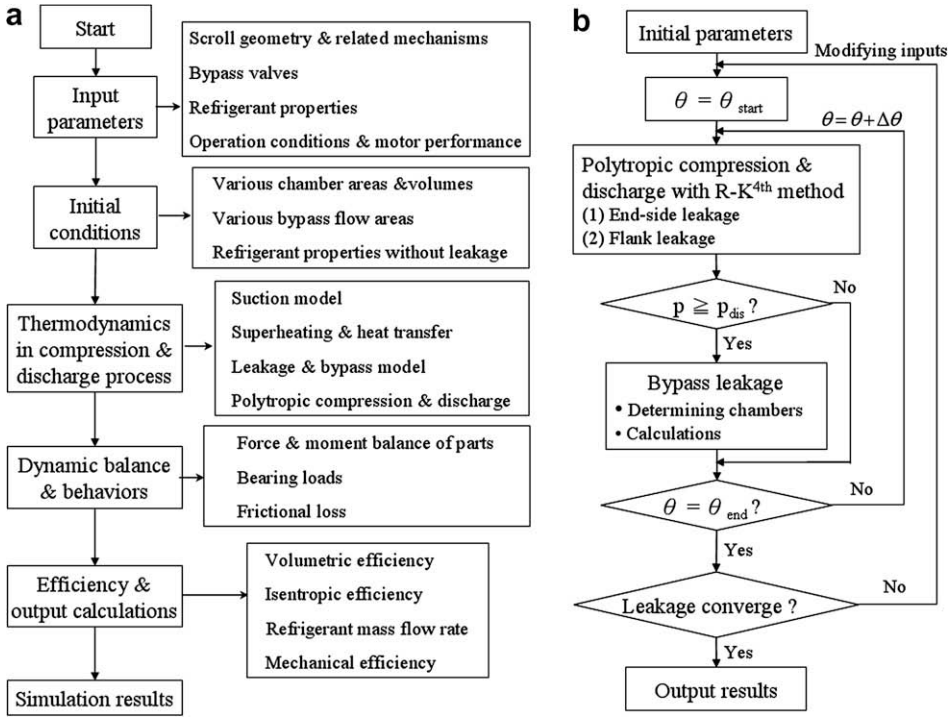

Fig. 3. The flowchart of the STC package (a) simulation process (b) leakage and bypass model.

than the pressure of the discharge chamber (p_{dis}), the bypass action occurs. Then the bypass flow can be calculated as leakage flow in the model. The 4th R–K method was the solution with convergent criterion as follows:

$$\frac{|\dot{m}_{l,p} - \dot{m}_{l,c}|}{\dot{m}_{l,c}} < CC_1 \tag{25}$$

3.3. Outputs

Three outputs used in the follow-up sections are stated as follows:

(1) Volumetric efficiency:

$$\eta_V = \frac{\dot{m}_{s,h} - \dot{m}_l}{\dot{m}_s} \tag{26}$$

(2) Isentropic efficiency:

$$\eta_C = \frac{P_{adiabatic}}{P_{motor}} \tag{27}$$

(3) Refrigerant mass flow rate:

$$G = \eta_V \times (V_s \times \rho_s \times \omega_{motor}) \tag{28}$$

4. Results and discussion

A CO_2 STC product is used for the simulation. The scheme of the STC and design of the bypass holes are shown in Fig. 4. The geometric parameters of the scroll pairs and bypass holes are displayed in Table 1. It can be seen that bypass hole 1 and bypass hole 2 are related to the outer involute and bypass hole 1′ and bypass hole 2′ to the inner involute. Five operating conditions for the simulation are used and the details are shown in Table 2.

The behavior of bypass holes can determine how long the holes would be exposed to the orbiting scroll during one orbiting cycle, however, the actual bypass action only occurs when the pressure in the chambers is greater than the pressure in the discharge chamber. Furthermore, thermodynamic calculation can estimate the amount of bypass flow rate.

4.1. Effect of bypass valves behavior

4.1.1. Bypass holes 1 and 2

Fig. 5 shows the change of uncovered area of the four bypass holes. It can be seen that the bypass hole 1 initially opened in chamber 2 and is covered by the orbiting scroll from 180° to 256°. Afterward, it opens in chamber 3 up to the end of the orbiting cycle. The bypass hole 2 is uncovered in chamber 2 from 0° to 20°, and is covered up to 66°. Then it appeared again in chamber 3 and remains there toward the end of the cycle. Fig. 6a illuminated that the two bypass holes may take effect in chamber 2 only from 720° to 797° (discharge angle) during the whole orbiting cycle, and after that, chamber 2 reaches the discharge stage. Similarly, chamber 3 also has a stage from 360° to 426° where the bypass holes were closed.

For chamber 2, the discharge angle of the scroll pairs must be considered. Since after the discharge angle, chamber 2 will communicate with chamber 1 and proceed to the discharge process. Therefore, if the discharge angle is appropriate, chamber 2 can avoid over-compression completely during the orbiting cycle. The discharge angle, 797°, is inside the useful acting interval of the bypass hole 1 (0°–180°), so the design is good for chamber 2.

For chamber 3, discharge angle does not interfere with bypass action, hence it merely needs to design bypass holes that can appear during the orbiting cycle. However, Fig. 6a shows that there are no bypass holes that open in chamber 3 from 360° to 426°. Though the interval is not very long, it is possible to cause over-compression in chamber 3. Besides, chamber 3 inhales refrigerant from the suction chamber. If too much liquid refrigerant flows into chamber 3, it could arise liquid slugging because of no bypass during the interval. It implies that the design of bypass holes in chamber 3 must be improved further.

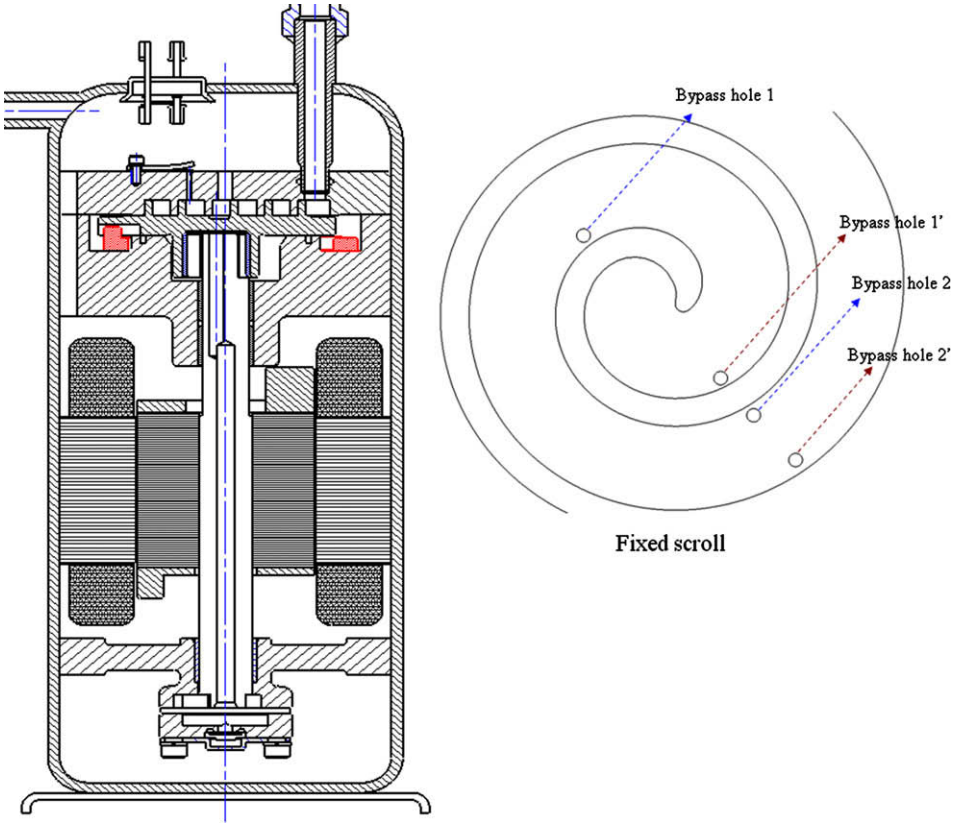

Fig. 4. The scheme of the STC and design of bypass holes on the fixed scroll.

Table 1
Parameters of the STC

Parameters	Value
Basic circle radius (r_b) (mm)	1.91
Thickness of the scroll (t) (mm)	3
Roll angle of the scroll (ϕ_r) (degree)	990
Height of the scroll (h) (mm)	4.27
Involute angle of bypass hole 1 (ϕ_{o_a}) (degree)	234
Radius of bypass hole 1 (r) (mm)	0.73
Distance of bypass hole 1 (d) (mm)	1.21
Involute angle of bypass hole 1′ (ϕ_{o_a}) (degree)	402
Radius of bypass hole 1′ (r) (mm)	0.73
Distance of bypass hole 1′ (d) (mm)	1.34
Involute angle of bypass hole 2 (ϕ_{o_a}) (degree)	407
Radius of bypass hole 2 (r) (mm)	0.73
Distance of bypass hole 2 (d) (mm)	0.92
Involute angle of bypass hole 2′ (ϕ_{o_a}) (degree)	770
Radius of bypass hole 2′ (r) (mm)	0.73
Distance of bypass hole 2′ (d) (mm)	1.57

Table 2
STC operating conditions

Refrigerant	CO_2		
	Suction pressure (MPa)	Discharge pressure (MPa)	Motor revolution (RPM)
Condition 1	3.67	10.44	2400
Condition 2	4.37	10.59	2892
Condition 3	3.25	11.19	3180
Condition 4	2.82	10.79	4200
Condition 5	4.5	11.06	2892

4.1.2. Bypass hole 1′ and 2′

Returning to Fig. 5 again, bypass hole 1′ is initially open in chamber 2′ and closed after 194°. At 260°, it is opened again in chamber 3′. A similar trend occurs to bypass hole 2′, which is opened initially in chamber 3′ and closed at 180°. After 260°, the hole is uncovered again in the next chamber (suction chamber).

As shown in Fig. 6b, chamber 2′ also can retain no over-compression during the cycle. For chamber 3′, it can be seen that from 540° to 620°, bypass holes are covered, and if the refrigerant in chamber 3′ is over-compressed, there is no passage to bypass it. The design of bypass holes in chamber 3′ may cause serious effects because generally speaking, over-compression occurs at the middle or later interval in outer chambers and at the early interval in inner chambers during a cycle. Hence, the possibility of over-compression in chamber 3′ may occur during 540°–620° because of the lack of bypass effect.

Therefore, different geometrical designs could produce different design requirements for the bypass holes. Geometrically, the major consideration is to design bypass holes which have longer uncovered intervals during an orbiting cycle.

4.2. Effect of bypass valves in thermodynamics

4.2.1. Effects with and without bypass action

Five conditions originated from JRAIA (Japan Refrigeration and Air Conditioning Industry Association) JRA4050:2005 were simulated with and without bypass action. Fig. 7 shows the compared simulation results in G, η_V and η_C of the STC with and without bypass action. It can be seen that G and η_V have hardly been influenced by bypass action but η_C, which is related to the power consumption of the compression process, changes fiercely and depends on various operating conditions. Improvement for bypass action in η_C at conditions 2 and 5 are almost 10% and 6% at condition 1, which implies the importance of the bypass action, even though at conditions 3 and 4, a lesser improvement of 2.5% was found. The observations above explain the necessity of designing

bypass valves in varied pressure ratio STC for more efficient and power-saving purposes.

4.2.2. Variation of pressure inside the compression chambers

Take notice of Figs. 5 and 6 again. Chambers 3 and 3′ are symmetrical with the same volume and the same change rate of volume during an orbiting cycle. The same conditions hold for chambers 2 and 2′. If bypass holes are designed inappropriately, they could produce pressure differences between the symmetrical chambers if bypass action occurs. Though the amount is small, the difference could affect the dynamic balance of scroll pairs and other mechanical components in STC [14]. For this reason, the

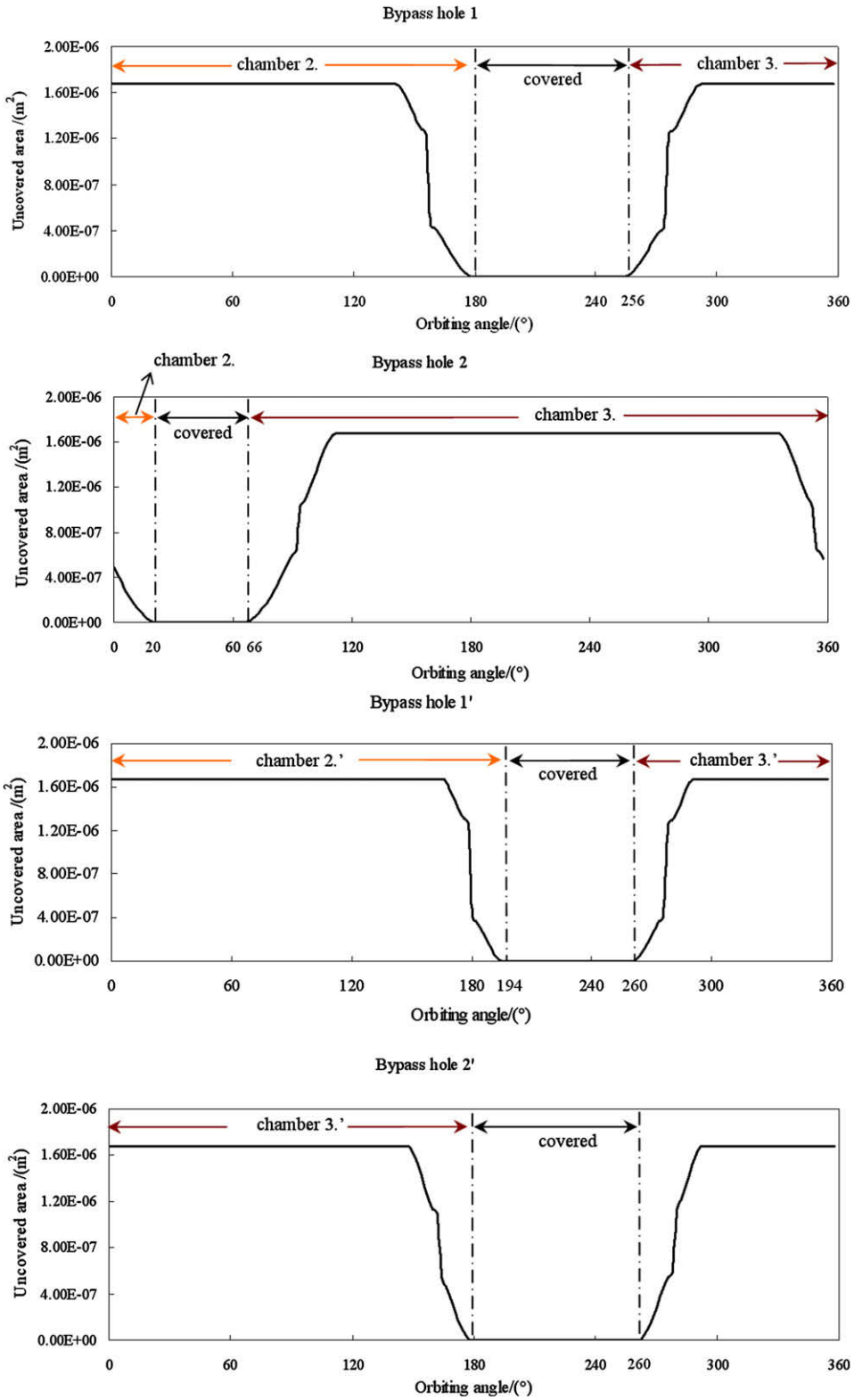

Fig. 5. Change of the uncovered area of bypass holes during an orbiting cycle.

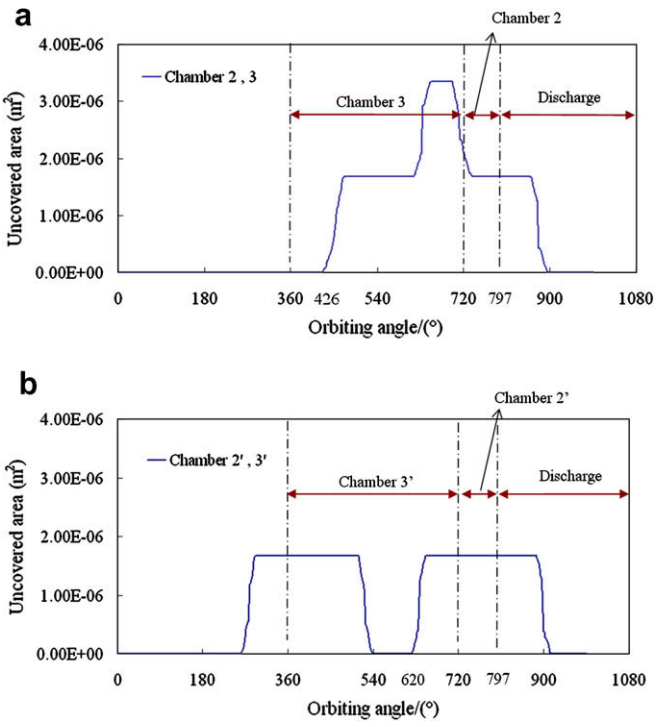

Fig. 6. Uncovered area of bypass holes in (a) chambers 2 and 3 (b) chambers 2′ and 3′.

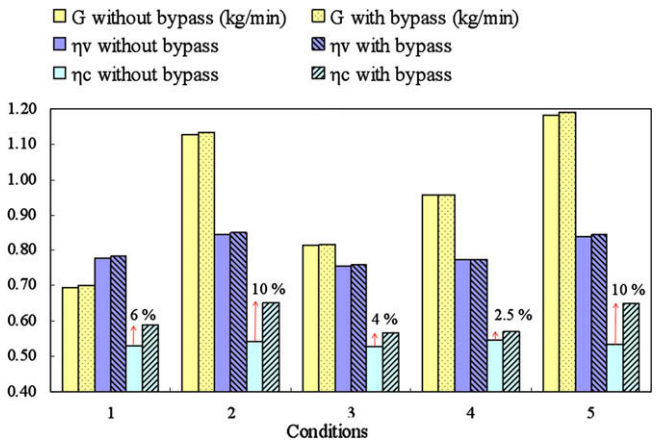

Fig. 7. Prediction of performance with and without bypass action of G, η_V and η_C.

design of bypass holes should make bypass action occurs at the same interval as far as possible in symmetrical chambers during a cycle and uncovered areas should close to equal.

Fig. 8 presents the simulation results of the pressure variations inside the compression chambers with and without bypass action. Through Figs. 6 and 8, it can be seen that the design of the four bypass holes can completely prevent over-compression during the orbiting cycle under these five conditions. The pressure discrepancies between chambers 2, 3 (Fig. 8a) and chambers 2′, 3′ (Fig. 8b)

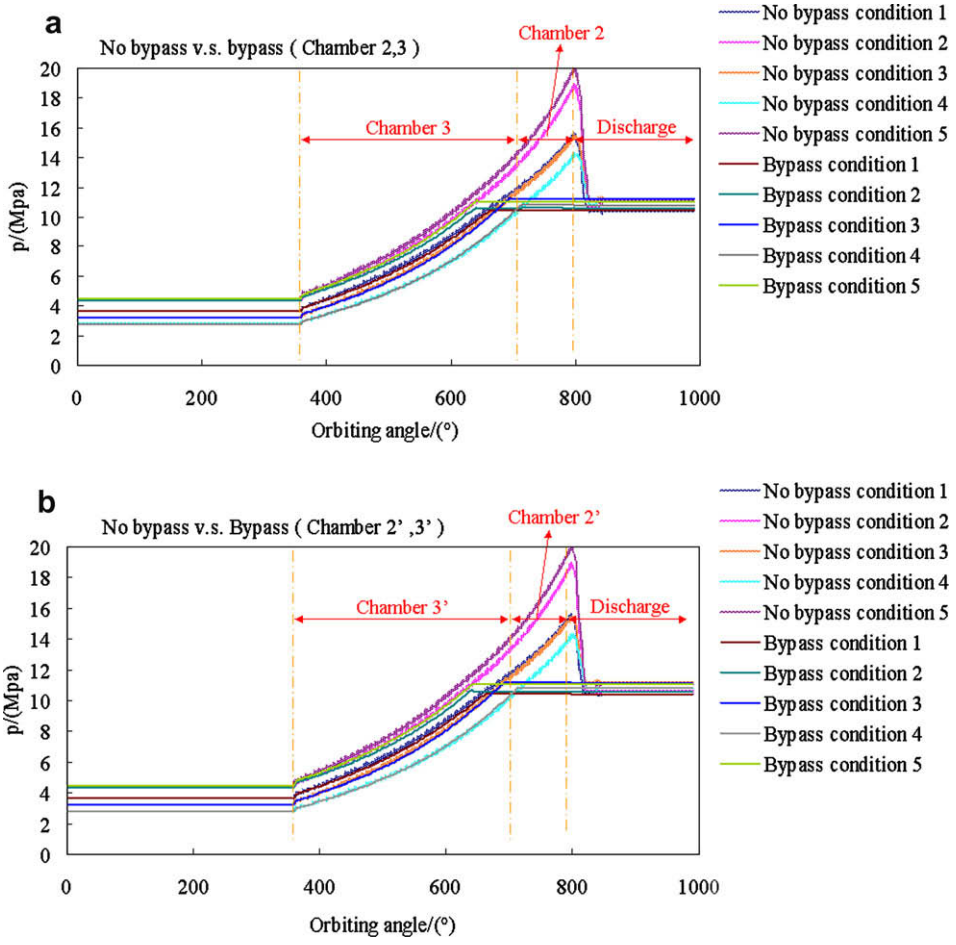

Fig. 8. Prediction of pressure variation with and without bypass valves (a) chambers 2, 3 (b) chambers 2′, 3′.

Table 3
Comparison between simulation and experimental results of G, η_V and η_C

Refrigerant	CO_2								
	G (kg/min)			η_V			η_C		
	Simulation	Experimental	Error (%)	Simulation	Experimental	Error (%)	Simulation	Experimental	Error (%)
Condition 1	0.7	0.721	−2.9	0.782	0.8	−2.3	0.59	0.59	0.0
Condition 2	1.134	1.125	0.8	0.85	0.84	1.2	0.651	0.64	1.7
Condition 3	0.818	0.845	−3.2	0.759	0.78	−2.7	0.566	0.57	−0.7
Condition 4	0.956	0.973	−1.7	0.773	0.78	−0.9	0.571	0.56	2.0
Condition 5	1.191	1.186	0.4	0.845	0.84	0.6	0.648	0.64	1.3

during the cycle are small, so the influence to dynamic balance can be neglected. However, the explanation cannot guarantee other operating conditions, because for chamber 3, bypass holes do not open during 360°–426° (Section 4.1.1) and for chamber 3′ do not open during 540°–620° (Section 4.1.2) of the orbiting cycle. Besides, the liquid slugging may occur in chamber 3. Hence, the design of current STC in the study can be further improved by using optimum method to determine better bypass holes for varied operating conditions.

4.2.3. Verification of bypass action

The simulation results were validated through the experimental apparatus which was developed by ITRI in cooperation with SINTEF [15,16]. A CO_2 STC product for heat pump system was installed in the testing apparatus, as a sample. The compared results are shown in Table 3. It was found that the models conform to the experimental results very well and the relative errors for these three results (G, η_V and η_C) are −3.2% to 0.8%, −2.7% to +1.2%, −0.7% to +2%, respectively. The models provided in the study can predict the performance with bypass action accurately.

5. Conclusions

The study has constructed a bypass mechanism mathematical model for preventing over-compression and liquid slugging inside the chambers of STC. Five aspects of the research are summarized below:

(1) The change of uncovered areas of bypass holes can be derived through the whole orbiting cycle of the developing STC by using coordinate transformation and some numerical schemes. Then the open and closed interval and corresponding chambers are also determined.
(2) The model is integrated into the compression and discharge processes of a comprehensive STC simulation package that can predict general efficiencies and performance.
(3) The model has been simulated under five specified operating conditions with and without bypass action and its accuracy has been validated by the experimental testing apparatus for a developing CO_2 STC product. It was found that the STC in this study with bypass valves increases 2.5% to 10% in isentropic efficiency and volumetric efficiency is scarcely affected.
(4) Pressure variations inside the chambers can also be viewed from the simulation results. It was found that the design of the bypass holes in the study can avoid over-compression completely inside the compression chambers under the five operating conditions. However for other different conditions, over-compression may occur because an interval (540°–620°) with covered bypass hole in chamber 3′ exists during the orbiting cycle. In addition, liquid slugging probably occurs at the initial stage (360° to 426°) in chamber 3.
(5) When exploiting a STC product for varied pressure ratio, the bypass valves model presented in the research is a useful tool that can determine whether the design is suitable or not for specific operating conditions. In addition, it can be further combined to an optimization tool to obtain new designs for particular conditions.

Acknowledgement

The authors would like to express gratitude for financial support from the Energy and Environment Research Laboratories, Industrial Technology Research Institute in Taiwan.

References

[1] C. Schein, R. Radermacher, Scroll compressor simulation model, Journal of engineering for gas turbines and power, Transactions of the ASME 123 (2001) 217–225.
[2] A. Murayama, N. Uchikawa, R. Kuroshima, H. Kuno, T. Arata, M. Shiibayashi, Scroll compressor with valid port for each compressor chamber, US Patent Number: 4,818,195, Date of Patent: April 4, 1989.
[3] K. Fuji, K. Sano, T. Morimoto, S. Hase, S. Yamamoto, K. Sawai, H. Ashitani, S. Yamada, Scroll compressor having bypass valves, US Patent Number: 5,855,475, Date of Patent: January 5, 1999.
[4] I. Tsubono, M. Takabayashi, I. Hayase, K. Inaba, K. Sekiguchi, K. Oshima, A. Shimada, T. Akizawa, Scroll compressor having a valved back pressure chamber and a bypass for overcompression, US Patent Number: 6,769,888, Date of Patent: August 3, 2004.
[5] T. Morimoto, S. Yamamoto, S. Hase, S. Yamada, N.Ishii, Development of a high SEER scroll compressor, in: Purdue International Compressor Engineering Conference Proceedings, 1996, pp. 317–322.
[6] Y.C. Chang, C.E. Tsai, C.H. Tseng, G.D. Tarng, L.T. Chang, Computer simulation and experimental validation of scroll compressor, in: Purdue International Compressor Engineering Conference Proceedings, 2004, p. C016.
[7] E. Morishita, M. Sugihara, T. Nakamura, W. Works, Scroll compressor analytical model, in: Purdue International Compressor Engineering Conference Proceedings, 1984, pp. 487–495.
[8] Y. Chen, N.P. Halm, E.A. Groll, J.E. Braun, Mathematical modeling of scroll compressors—part I: compression process modeling, International Journal of Refrigeration 25 (2002) 731–750.
[9] J.J. Nieter, D.P. Gagne, Analytical modeling of discharge flow dynamics in scroll compressors, in: Purdue International Compressor Engineering Conference Proceedings, 1992, pp. 85–94.
[10] R.L. DeBlois, R.C. Stoeffler, Instrumentation and data analysis techniques for scroll compressors, in: Purdue International Compressor Engineering Conference Proceedings, 1988, pp. 182–188.
[11] E.W. Lemmon, M.O. McLinden, M.L. Huber, REFPROP 7.0, NIST, MD, USA.
[12] B. Wang, W. Shi, Xi. Li, Qi. Yan, Numerical research on the scroll compressor with refrigeration injection, Applied Thermal Engineering 28 (2008) 440–449.
[13] T. Yanagisawa, T. Shimizu, Leakage losses with a rolling piston type rotary computer II: leakage losses through clearances on rolling piston faces, International Journal of Refrigeration 8 (3) (1985) 152–158.
[14] T. Yamada, S. Yamamoto, S. Sawai, K. Kohayakawa, T. Hase, S. Ashitani, Scroll gas compressor having asymmetric bypass holes, US Patent Number: 6,273,691, Date of Patent: August 14, 2001.
[15] T. Skiple, H. Rekstad, A. Hafner, CO_2 technology transfer, Technical Report No. 061206151146, SINTEF Energy Research, 2006.
[16] H. Rekstad, Technical specifications of CO_2-compressor test rig, Technical Report No. 03082192212, SINTEF Energy Research, 2007.